IEEE Transactions on Transportation Electrification, Volume 9, Issue 1, March 2023, pp. 609-621
DOI:10.1109/TTE.2022.3190167

A New Topology for Electric All-Terrain Vehicle Hybrid Battery Systems Using Low-Frequency Discrete Cell Switching

You Gong, Daniel J. Auger, *Senior Member, IEEE*,
Abbas Fotouhi, *Senior Member, IEEE* and Christoper J. Hale

Abstract

his paper presents an investigation into the feasibility of a novel discrete-switched topology for an electric all-terrain vehicle (e-ATV) hybrid battery system that avoids expensive and bulky DC-DC converters using a simpler discrete-switched structure together with an intelligent low-frequency switching algorithm. Hardware is simplified at the expense of more complex control. The algorithm switches cells in and out of series strings, based on their state of charge relative to other cells in the pack and the power being drawn from the pack. The principles are demonstrated using a simulated model combining lithium-titatate-oxide (LTO) and lithium-ion-phosphate (LFP) cells together in an e-ATV battery pack. Despite its simplicity, the intelligent switching algorithm, successfully allocates power to different elements of the battery and ensures that state of charge remains broadly balanced throughout discharge, with the pack ending up in good balance: the LFP cells are in balance to within 0.01% of each other, and the LTO cells within 0.1% of each other. While the paper focuses on the essential feasibility of the concept, it also identifies future research for including thermal effects, uncertainties in state estimation, cell ageing and non-uniformly, and consideration of other powertrain components, e.g. motor and power electronics.his paper presents an investigation into the feasibility of a novel discrete-switched topology for an electric all-terrain vehicle (e-ATV) hybrid battery system that avoids expensive and bulky DC-DC converters using a simpler discrete-switched structure together with an intelligent low-frequency switching algorithm. Hardware is simplified at the expense of more complex control. The algorithm switches cells in and out of series strings, based on their state of charge relative to other cells in the pack and the power being drawn from the pack.

Manuscript submitted on March 18, 2022. This work was partially supported by Innovate UK under grants number 48727 and 10017550.

Y. Gong, D. J. Auger and A. Fotouhi are with the School of Aerospace, Transport and Manufacturing Ltd, Cranfield University, UK.

C. J. Hale is with Upgrade Technology Engineering, Potters Bar, UK

The principles are demonstrated using a simulated model combining lithium-titatate-oxide (LTO) and lithium-ion-phosphate (LFP) cells together in an e-ATV battery pack. Despite its simplicity, the intelligent switching algorithm, successfully allocates power to different elements of the battery and ensures that state of charge remains broadly balanced throughout discharge, with the pack ending up in good balance: the LFP cells are in balance to within 0.01% of each other, and the LTO cells within 0.1% of each other. While the paper focuses on the essential feasibility of the concept, it also identifies future research for including thermal effects, uncertainties in state estimation, cell ageing and non-uniformly, and consideration of other powertrain components, e.g. motor and power electronics.T

I. Introduction

Battery systems play a vital role in the technological development of electric vehicles (EVs). To be viable in the market, the battery system in an EVs must provide adequate safety, high energy density, high power density, long lifespan and low cost [1], [2]. At present, the post popular battery chemistries for EVs are variants of lithium-ion. Each of the battery chemistries in the Li-ion battery family has distinct advantages and weaknesses [3].

TABLE I
Comparison of characteristics of Li-ionBatteries [2]–[10]

Material	Specific energy [Wh/kg]	Charge C-rate	Discharge C-rate	Safety	Cycle life
LCO	110–190	0.5	1	Low	500–1000
LMO	100–120	1	2	Medium	1000
NCA	100–150	1	2	Low	2000–3000
NMC	100–170	0.5	1	Medium	2000–3000
LFP	90–115	0.5–1	1–5	High	3000
LTO	60–75	5–10	10	High	5000–20000

A comparison of Li-ion battery characteristics is shown in Table I. Lithium-iron-phostphate (LFP) batteries are safe and, have good specific energy and a relatively low price [4]–[6]. However, LFP is not particularly strong in terms of specific power (charge and discharge C-rate) and it is vulnerable to rapid battery degradation under high power demand [2], [7]. By contrast, lithium-titanate-oxide (LTO) has fast charge/discharge ability, wide working temperature ($-35°C \sim 55°C$), a long life-span (approximately 20 000 cycles) and excellent safety [3], [5], [8]. Nevertheless, low specific energy hinders its large-scale application [9]. Other battery chemistries such as lithium-nickel-manganese-cobalt (NMC),lithium-manganese

spinel (LMO), lithium-nickel-cobalt-aluminum (NCA), and lithium cobalt oxide (LCO) batteries have a high specific energy, but are less satisfactory in terms of specific power, safety and lifespan. There is no single battery chemistry that is 'best' in all categories. The battery designer can either select a single chemistry that is 'good enough', and this is the most widespread approach today. However, an alternative approach is a mixed-chemistry battery, using a hybrid energy storage system (HESS) with two types of energy storage, has been proposed to prolong the service life of the system and better manage the conflicting requirements of energy and power density [11].

In the literature, a common approach to EV HESS is to combine supercapacitors and li-ion batteries [12]–[14]. Although they are relatively bulky, supercapacitors have higher specific power and better cycle life than li-ion batteries [15], [16]. A HESS like this uses supercapacitors as an auxiliary power source to absorb the power peaks and allow the battery to operate with a lower discharge/charge rates. There are three typical topologies in the literature: passive, semi-active and active [13], [17]. The difference between them is whether the DC/DC converters are utilised to regulate the power allocation (passive and semi-active topology) and the number of DC/DC converters in the system (semi-active and active topology). For each topology, there exist studies on the sizing optimisation and management strategy for optimized weight, cost and minimization of battery degradation. However, due to supercapacitors' poor specific energy (3.5 $\sim$ 4.5 Wh/kg), supercapacitors in the HESS are only operated in urban environments or short-range driving, but have less effective in medium and long-distance driving scenarios [11], [18].

LTO batteries offer – qualitatively at least – similar advantages to supercapacitors: they support fast charge/discharge, have a wide working temperature envelope, and last for a high number of cycles. However, compared to supercapacitors, LTO batteries are cheaper and have higher specific energy. Hybrid battery systems combining multiple battery types were proposed in [19], where different chemistry batteries in the system are used separately under various power requirements. High and low power demands are provided by the chemistry battery with high and low specific power, respectively. A hybrid battery system (HBS) with LFP and LTO batteries in the electric buses has been proposed in [20], where a passive topology is used with the two battery types working simultaneously, with the allocation of power depending on the inherent characteristics of two batteries. These two systems have the advantages of simple structure and low cost, but power allocation of the battery systems cannot be regulated. An HBS using individually switched modules has been proposed in [21], where a module comprises a plurality of series and parallel battery cells. However, it did not

demonstrate methods of flexible power allocation regulation and SOC balancing. In [22], a deep reinforcement learning-based energy management strategy for a HBS was proposed, but this method also used a semi-active topology. Another solution is to use a DC/DC converter in each module to manage each module current [23]; this solution has flexible current regulation for each module, but it also has to compromise on hardware complexity and cost.

Approaches to flexible power allocation with a semi-active topology has been proposed in the literature [24], [25]: DC/DC converters can be used to regulate the power allocation between LTO and LFP batteries, with control strategies based on either a low-pass filter of fuzzy logic. These effectively completely decouple the physics and chemistry of the battery elements from the power allocation strategy. However, these strategies require the use of high power DC/DC converters, which, while effective, does adversely affect system cost, weight and bulk. Consequently, existing HBSs have following drawbacks: 1) existing passive topologies have simple structures and low cost, but cannot flexibly regulate power allocation. 2) existing semi-active and active topologies can flexibly allocate power, but they are expensive and bulky. It is interesting to consider whether a similar topology could use cheaper (if less capable) power electronics to achieve a less-perfect but still 'reasonable' balance between allocation flexibility and system cost.

The contributions of this study are as follows:

1) A novel HBS topology is proposed, using a discrete-switched structure to regulate power allocation between two types of batteries. The structure switches cells in and out of series strings, based on their state of charge relative to other cells in the pack and the power requirement, as shown in Fig. 2. (More detail will be presented in section II.)
2) A benchmark control algorithm using high-level rules with lower-level near-optimal control is demonstrated.
3) The costs are compared to a conventional hybrid battery system and shown to be lower.

For this study, two battery chemistries within the Li-ion battery family are chosen, namely LFP and LTO batteries have been selected for this study. These were chosen with an industrial application in mind: they are safe, and they have complementary advantages in specific power, energy, and lifespan. However, the method is potentially suitable for any similar situation with two or more battery types, or indeed other electrical energy storage systems.

To the best of the authors' knowledge, there are no existing systems with this topology. Battery systems derived from this approach are being developed as part of publicly-funded research projects in the UK, of which the authors are part. [26], [27].

The paper is organised as follows. In Section II, the novel topology is presented and illustrated and the relative costs are explored. In Section III, the battery cell and the system of the topology is modelled. In Section IV, referring to existing management strategies, the energy management strategy for the system is proposed, including power allocation and cell balancing. In Section V, simulation results are presented and analysed to verify capabilities of power allocation and SOC balancing. Finally, in Section VI, this paper is concluded.

II. The Discrete-Switched Topology

Conventional HBS topologies, as explored in [13], [17], [28], are shown in Fig.1. Battery sub-packs are connected to high power DC/DC converters in conventional topologies. By contrast, the discrete-switched topology has a reasonable switch arrangement to achieve power regulation instead of the DC/DC converters in the conventional topologies.

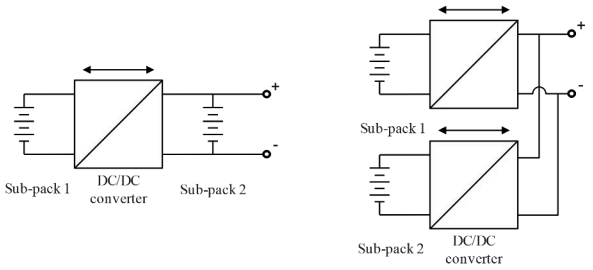

(a) Semi-active HBS with one DC/DC converter **(b) Active HBS with two DC/DC converters**

Fig. 1. Conventional HBS topologies

Fig. 2 illustrates a topology of the proposed HBS for the hybrid LFP-LTO battery source. The LFP and LTO battery sub-packs are connected in parallel via sub-pack switches S_1 and S_2. Load current and voltage are I_L and V_L, respectively. The currents of the LFP and LTO battery sub-packs are I_1 and I_2, respectively. S_1 and S_2 control the connection and disconnection of two battery sub-packs to the load. In each battery sub-pack, a parallel string composed of battery cells in parallel and two switches is defined as a module. LFP and LTO sub-packs have M and N battery modules, respectively. Each module has two switches: main switch and bypass switch. These switches enable module cells to switch in and out of series strings in a sub-pack. Main switches are indicated as S_{ij1}, and bypass switches are indicated as S_{ij2}, where i is the battery type, $i = 1$ and $i = 2$ represent the LFP and LTO battery sub-packs, respectively, and j is the module number in battery sub-pack i. Voltage sensors are connected in each battery module, and current sensors are connected in each battery sub-pack.

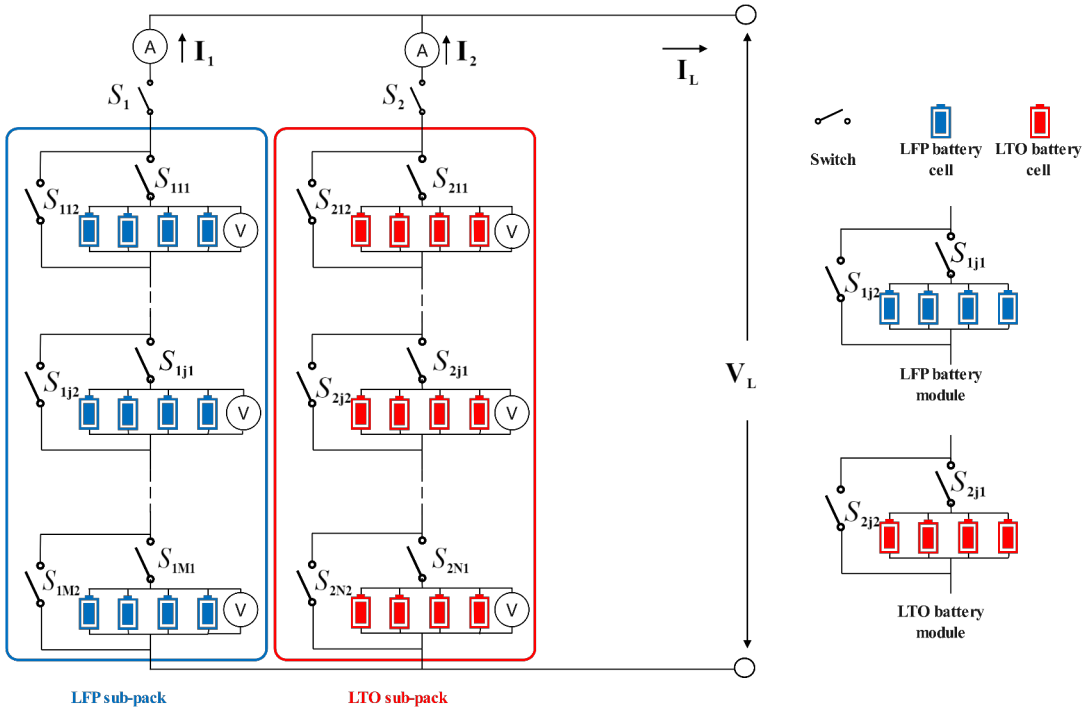

Fig. 2. The discrete-switched topology of the HBS with LTO and LFP batteries. LFP and LTO sub-packs have M and N battery modules, respectively. In this case study, LFP sub-pack has 113 serials and 12 parallels, and LTO sub-pack has 160 serials and 4 parallels.

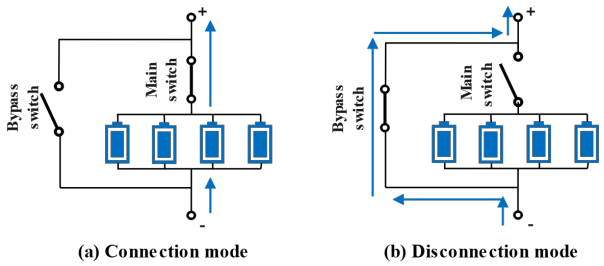

Fig. 3. Operation modes of a module (blue lines with an arrow represent current direction): (a) Connection mode, and (b) Disconnection mode.

The battery module structure and operation modes are shown in Fig. 3. A battery module has a main circuit and a bypass circuit. The main and bypass switches are on the main and bypass circuit, respectively, to control the connection and disconnection of the circuit. An interlock is applied between the two switches to avoid simultaneous switch-on or switch-off. Operation modes are manipulated by main and bypass switches, where each module contains two operation modes: ‘connection’ and ‘disconnection’. For the ‘connection’, the main switch is closed, and the bypass switch is opened; current can flow through the module, and it will

participate in the overall charging and discharging process. Conversely, for the 'disconnection', the switches have the opposite settings; current can still flow through the module via the low-resistance bypass circuit, but the battery's cells are disconnected. The cells within each module remain connected to each other as usual, enabling natural self-balancing to continue [29].

In a typical hybrid battery system, switching is done by pulse-width modulated DC-DC converters and must operate thousands of times a second and cope with the full voltage of the pack. This is not the case in the discrete-switched topology. The idea here is to use 'event based' switching based on driving power requirements and battery states. Switching also operates at or close to cell voltage (typically $2 - 4$ V).

To give an idea of likely cost, the costs of a conventional semi-active hybrid battery system are compared to the the costs of a this paper's proposed system – detailed in the case study in section V. The costs considered include a high power DC/DC converter and bypass structures for cell balancing with MOSFET switches [29]. The cost of a DC/DC is approximately £40.5/kW, and the semi-active system needs a DC/DC converter of about 50 kW [30]. Thus, the DC/DC converter is around £2025. The cost comparison is given in Table II. This shows that the power electronics used in a conventional system cost over £2200, but the proposed topology costs under £400; in the proposed topology, the MOSFET switching is comparable in cost and complexity to a 'standard' cell balancing system, and there there is no need for a full-voltage DC/DC converter.

TABLE II
COMAPARISON OF COSTS: PROPOSED SYSTEM VS CONVENTIONAL SEMI-ACTIVE TOPOLOGY
(DATA DERIVED FROM [30], [31])

Parameters	**Proposed topology**	**Conventional semi-active topology**
LFP series number	113	
LTO series number	160	
Switch price (£/per MOSFET)	0.7	
Switch number	548 (Module and sub-pack switches)	273 (Cell balancing switches)
Total switch price (£)	383.6	191.1
DC-DC converter price (£)	0	approx.2025
Total power electric price (£)	383.6	2216.1

There is, of course, a cost to pay in terms of operational complexity: a discrete-switched

topology will need a complex algorithm to decide which switches to operate and, as switching is discrete, it is unlikely that the exact 'optimal' conditions (details will be described in Section IV and V).

The first stage in designing a switching algorithm for the hybrid-switched topology is to mathematically describe such a system's behaviour. In the following section, we present the development of an appropriate model set for addressing this.

III. Model Development

A. Cell-level modelling

The cells within the battery are modelled using first-order RC equivalent-circuit networks, i.e. state-dependent 'Thevenin' models; the format is illustrated in Fig. 4. Here, $V_{oc,\text{cell}}$ is cell open-circuit voltage (V), $R_{o,\text{cell}}$ is cell internal resistance (Ω), $R_{p,\text{cell}}$ and $C_{p,\text{cell}}$ are a 'polarisation' resistance (Ω) and capacitance (F) describing transient response; $V_{p,\text{cell}}$ is the'polarisation' voltage (V), and V_{cell} is the terminal voltage (V) of the cell. The parameters of the LFP and LTO cells are listed in Table III [20], [32]–[34]. A discharge-positive current convention is used. The parameters of the cells are modelled as being dependent on their state of charge, and follow the trends shown in Fig. 5 [32], [35]. The dynamic behaviours of the battery cell is described by (1):

$$\mathcal{S}_{\text{cell}} \begin{cases} \dot{\chi}_{\text{cell}}(t) = -\dfrac{1}{3600\,Q_{\text{cell}}}\, I_{\text{cell}}(t) \\ \dot{V}_{p,\text{cell}}(t) = -\dfrac{1}{R_{p,\text{cell}}\,C_{p,\text{cell}}} V_{p,\text{cell}}(t) + \dfrac{1}{C_{p,\text{cell}}}\, I_{\text{cell}}(t) \\ V_{\text{cell}}(t) = \; V_{oc,\text{cell}} - V_{p,\text{cell}}(t) - R_{o,\text{cell}}\, I_{\text{cell}}(t) \end{cases} \tag{1}$$

where χ_{cell} is the state of charge for the battery cell (normalised from 0 to 1), I_{cell} is the current through the cell (A), and Q_{cell} is the cell capacity (Ah).

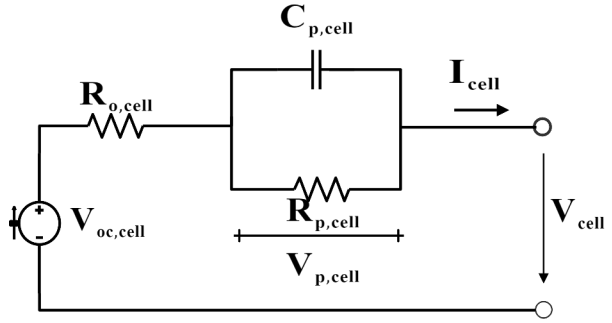

Fig. 4. First-order RC model of LFP and LTO

TABLE III

BASIC PARAMETERS OF THE SELECTED LFP AND LTO BATTERY CELLS

Battery type	**LFP**	**LTO**
Nominal voltage (V)	3.2	2.3
Capacity (Ah)	10	13
Maximum discharge rate (C)	1	10
Maximum charge rate (C)	1	10
Cycle life (Cycle, 80% DOD)	3000	30000

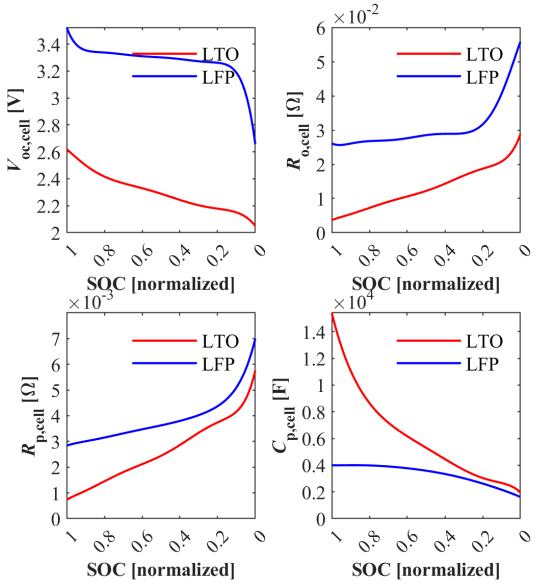

Fig. 5. Variation of case-study cell parameters with respect to state of charge (25°C) [32], [35]

B. Battery Sub-pack and System Model

The battery sub-packs switches and the module operation modes are represented by piece-wise function as (2) to explain conveniently.

$$S_i = \begin{cases} 1 & \text{connection} \\ 0 & \text{disconnection} \end{cases}$$
$$M_{(i,j)} = \begin{cases} 1 & \text{connection mode} \\ 0 & \text{disconnection mode} \end{cases} \tag{2}$$

where subscript i and j indicate the same meaning as Fig. 2. S_i represent the sub-pack switch i, and $M_{(i,j)}$ represent the module operation mode of the j module in the battery sub-pack i.

It is assumed that the battery cells in each module are almost uniform. (This is not necessarily true in practice, and non-uniformity will be explored in future work.) In a module, the relationship between a battery module and the cells made up of the module is depicted as (3).

$$\begin{aligned} Q_{(i,j)} &= Q_{\text{cell}} N_p \\ V_{oc,(i,j)} &= V_{oc,\text{cell}} \\ R_{o,(i,j)} &= \frac{R_{o,\text{cell}}}{N_p} \\ R_{p,(i,j)} &= \frac{R_{p,\text{cell}}}{N_p} \\ C_{p,(i,j)} &= C_{p,\text{cell}} N_p \end{aligned} \tag{3}$$

where N_p is the number of cells in the module, $Q_{(i,j)}$ is the module capacity, $V_{oc,(i,j)}$ is module terminal voltage, $R_{o,(i,j)}$ is module internal resistance, $R_{p,(i,j)}$ and $C_{p,(i,j)}$ are the module polarisation resistance and capacity for the module transient responds, respectively. Since the impact of module operation mode on states of the module is reflected in the current throughout the module, the state of the module can be expressed as (4) based on (1).

$$\begin{aligned} \dot{\chi}_{(i,j)} &= -\frac{M_{(i,j)} I_i}{3600 Q_{(i,j)}} \\ \dot{V}_{p,(i,j)} &= -\frac{V_{p,(i,j)}}{R_{p,(i,j)} C_{p,(i,j)}} + \frac{M_{(i,j)} I_i}{C_{p,(i,j)}} \\ E_{(i,j)} &= V_{oc,(i,j)} - V_{p,(i,j)} \end{aligned} \tag{4}$$

where the I_i is the current throughout sub-pack i, $\dot{\chi}_{(i,j)}$ is the differential of the module SOC, and $E_{(i,j)}$ is the transient electromotive force of the module. $M_{(i,j)} I_i$ is the current through the battery module. For the battery sub-pack i, the module states and switches can be depicted as vectors, as shown in (5).

$$\begin{aligned} \vec{\boldsymbol{M}}_{\boldsymbol{i}} &= [M_{(i,1)}, \quad \ldots, \quad M_{(i,j)}, \quad \ldots, \quad M_{(i,n)} \ ] \\ \vec{\boldsymbol{E}}_{\boldsymbol{i}} &= [E_{(i,1)}, \quad \ldots, \quad E_{(i,j)}, \quad \ldots, \quad E_{(i,n)} \ ] \\ \vec{\boldsymbol{R}}_{\boldsymbol{i}} &= [R_{o,(i,1)}, \quad \ldots, \quad R_{o,(i,j)}, \quad \ldots, \quad R_{o,(i,n)}] \end{aligned} \tag{5}$$

where n is number of modules in a sub-pack, $\vec{\boldsymbol{M}}_{\boldsymbol{i}}$ is the vector of operation modes of the modules in a sub-pack, $\vec{\boldsymbol{E}}_{\boldsymbol{i}}$ is the vector of transient electromotive forces of the modules in a sub-pack, $\vec{\boldsymbol{R}}_{\boldsymbol{i}}$ is the vector of the internal resistances of the modules in a sub-pack. Thus, the

transient electromotive force E_i and internal resistance R_i of sub-pack i can be represented as (6).

$$\begin{aligned} E_i &= \vec{\boldsymbol{M}}_{\boldsymbol{i}} \vec{\boldsymbol{E}}_{\boldsymbol{i}}^{\,T} \\ R_i &= \vec{\boldsymbol{M}}_{\boldsymbol{i}} \vec{\boldsymbol{R}}_{\boldsymbol{i}}^{\,T} \end{aligned} \tag{6}$$

where E_i and R_i are the transient electromotive force and the internal resistance in sub-pack i.

In equation (6), transient E_i can be regulated by operating $\vec{\boldsymbol{M}}_{\boldsymbol{i}}$, but R_i is also changed with the change of $\vec{\boldsymbol{M}}_{\boldsymbol{i}}$. The essential objective for the system is to control $\vec{\boldsymbol{M}}_{\boldsymbol{i}}$ so that the power input and output of the two battery sub-packs can be reasonably allocated. Based on the equation (6) and Kirchhoff laws, the relationship between sub-packs and system level can be expressed as equation (7).

$$\begin{aligned} I_L &= \sum_{i=1}^{2} I_i \\ V_L &= V_i = E_i - I_i R_i \\ P_L &= V_L I_L = \sum_{i=1}^{2} P_i \end{aligned} \tag{7}$$

where I_L and V_L are load current and voltage (V), P_L is the total power demand of the system (W), and P_i is the output power of the battery pack i (W). To deduced the power allocation functions conveniently in the context, the symbols used in the functions are defined as (8).

$$\begin{aligned} I_s &= \sum_{i=1}^{2} \frac{S_i E_i}{2R_i} \\ R_s &= \left(\sum_{i=1}^{2} \frac{S_i}{R_i} \right)^{-1} \\ V_s &= I_s R_s \end{aligned} \tag{8}$$

During driving processes, it is worth noting that the S_1 and S_2 can not equal to 0 simultaneously, which is in line with the actual situation that the system must be connected to the load. Furthermore, the battery system power allocation satisfies (9) according to (7) and (8).

$$R_s I_L^2 - 2V_s I_L + P_L = 0 \tag{9}$$

Finally, load current I_L, load voltage V_L, sub-pack current I_i and power P_i can be solved by (7) and (9).

$$\begin{aligned} I_L &= I_s\,(1-\phi) \\ V_L &= V_s\,(1+\phi) \\ I_i &= \frac{E_i}{R_i} + \frac{V_s}{R_i}\,(1+\phi) \\ P_i &= -\frac{V_s^2}{R_i}\,(1+\phi)^2 + \frac{E_i V_s}{R_i}\,(1+\phi) \end{aligned} \tag{10}$$

where

$$\phi = \sqrt{1 - \frac{P_L}{I_s^2 R_s}}$$

Consequently, the power allocation can be expressed as (11).

$$\begin{aligned} P_1 &= f_1(\boldsymbol{X}_{\text{sys}}, \boldsymbol{U}_{\text{sys}}, P_L) \\ P_2 &= f_2(\boldsymbol{X}_{\text{sys}}, \boldsymbol{U}_{\text{sys}}, P_L) \end{aligned} \tag{11}$$

where $\boldsymbol{X}_{\text{sys}}$ is all states of the system from measurement and estimation, and the control input is $\boldsymbol{U}_{\text{sys}}$ including module modes and battery sub-pack switches. $\boldsymbol{X}_{\text{sys}}$ and $\boldsymbol{U}_{\text{sys}}$ can be expressed as (12).

$$\begin{aligned} \boldsymbol{X}_{\text{sys}} &= \{\vec{\boldsymbol{E}}_{\boldsymbol{1}}, \vec{\boldsymbol{R}}_{\boldsymbol{1}}, \vec{\boldsymbol{E}}_{\boldsymbol{2}}, \vec{\boldsymbol{R}}_{\boldsymbol{2}}\} \\ \boldsymbol{U}_{\text{sys}} &= \{\vec{\boldsymbol{M}}_{\boldsymbol{1}}, \vec{\boldsymbol{M}}_{\boldsymbol{2}}, S_1, S_2\} \end{aligned} \tag{12}$$

Thus, the power allocation between battery sub-packs on the different control inputs can be estimated through known power demand and system states.

IV. HBS Energy Management

A. Description

Section II and III have developed and modelled the discrete-switched topology. The overall control strategy for this system consists of a rule-based supervisory controller designed to achieve high-level aims, together with a low-level control algorithm designed to optimize performance in achieving the objectives of the supervisory rules. A filtration-based algorithm is then used to create a target reference for power allocation. A low-level controller to approximate this is then calculated optimally. This controller is intended as a benchmark, and also to be suitable for real-time execution on today's industry-standard hardware. A number of simplifying assumptions are made, such as reasonable homogeneity of cells and modules, uniform temperature distributions and the availability of accurate state of charge estimates. (In the conclusions, these are noted as areas for future work.)

Equations (11) and (12), describe how power allocation responds to switch positions described by the vectors $\vec{\boldsymbol{M}}_{\boldsymbol{1}}$ and $\vec{\boldsymbol{M}}_{\boldsymbol{2}}$ and the main sub-pack switches S_1 and S_2. The currents in the modules are determined by these switch positions and the current state of each cell in the battery. The module SOCs would unbalance without proper control, and a management strategy is need to achieve a desired outcome. A management strategy aims:

1) To flexibly allocate power between two battery sub-packs (providing similar capability to the semi-active or active HBSs), and
2) To keep module SOCs broadly balanced throughout operating processes.

Sub-pack currents and SOCs may need to be constrained according to the batteries' intended operating envelopes, e.g. to preserve lifespan. As the switches are discrete, the control algorithm to determine the instanteous values of $\vec{\boldsymbol{M}}_{\boldsymbol{1}}$ and $\vec{\boldsymbol{M}}_{\boldsymbol{2}}$ takes the form of an integer optimization control with inequality constraints. This is more complicated than the algorithms required for existing topologies.

The energy management for the proposed topology combines two control strategies to solve switching decisions: rule-based and filtration-based strategies. The filtration-based strategy is implemented to provide the power allocation reference. Through a low-pass filter, power demands with rapid fluctuations are filtered to smooth values, as power references of the LFP sub-pack. The control algorithm of subsection C will regulate $\boldsymbol{U}_{\text{sys}}$ to fit as close as possible to the power references, and the LTO sub-pack absorbs power peaks. However, only a filtration-based strategy cannot avoid the possibility of overcharging and over-discharging sub-packs. Thus, the rule-based strategy is mainly used to protect two battery sub-packs from overcharging or over-discharging. Therefore, the energy management is divided into two steps to implement. For the first step, the rule-based strategy decides the sub-pack switches S_1 and S_2 based on the LFP and LTO battery sub-packs SOCs. For the second step, the filtration-based strategy decides the module switches $\vec{\boldsymbol{M}}_{\boldsymbol{1}}$ and $\vec{\boldsymbol{M}}_{\boldsymbol{2}}$ when the two sub-packs coordinately work.

Rule-based energy management strategy is first adopted [13], [24], [25]. The detailed system operation modes for a driving process are demonstrated in Table IV, in which SOC_{LFP} and SOC_{LTO} (%) are the LFP and LTO battery sub-packs SOCs, respectively. SOC_{LFP} and SOC_{LTO} are average values of their module SOCs $\chi_{(i,j)}$ because module SOCs in a sub-pack remain broadly balanced, and it will be verified in later sections. In the overall driving process, the SOC_{LFP} and SOC_{LTO} are limited by more than 10% to protect the battery sub-packs from over-discharge at discharge modes, and they are restricted by less than 90% to avoid overcharge at regenerative braking modes [20], [24], [25]. Discharge modes I and II can

TABLE IV
THE OPERATION MODES FOR THE HBS IN DRIVING PROCESS

Operation mode	$SOC_{\mathrm{LFP}}(\%)$	$SOC_{\mathrm{LTO}}(\%)$	S_1	S_2	**LFP state**	**LTO state**
Discharge mode I	[0 10]	[0 100]	Off	On	Idle	Discharge
Discharge mode II	[10 100]	[0 10]	On	Off	Discharge	Idle
Discharge mode III	[10 100]	[90 100]	Off	On	Idle	Discharge
Discharge mode IV	[10 100]	[10 90]	On	On	Discharge	Discharge
Mechanical braking mode	[0 100]	[90 100]	Off	Off	Idle	Idle
Regenerative braking mode	[0 100]	[0 90]	Off	On	Idle	Charge

protect the LFP or LTO battery sub-packs from over-discharge. When the SOC_{LTO} exceeds 90%, only the LTO battery sub-pack provides the power to the load, and the system works in discharge mode III. This mode reduces frequently using the LFP battery sub-pack under the high-level SOC_{LTO} to improve its degradation. It is also beneficial to protect the LFP battery sub-pack during the 'cold start' of a vehicle. When the SOC_{LFP} and SOC_{LTO} are in the range of 10% $\sim$ 100% and 10% $\sim$ 90%, respectively, the two battery sub-packs are coordinated discharged to meet the power demand, so the system works in discharge mode IV. In this mode, the two battery sub-packs allocate the power demand depending on the power demand and SOC states to reduce the current throughout the LFP battery sub-pack and mitigate the influence of the high or pulse current on the LFP battery ageing [7], [12].

For braking modes, the LTO battery sub-pack absorbs the regenerative braking energy to avoid aggravating ageing due to recurrent charges to the LFP sub-pack during a driving process, ensuring that the LTO battery sub-pack is charging preferentially. The mechanical braking mode can be used to protect the LTO battery sub-packs from overcharge. Long-term recharging, e.g. from a stationary charger, is not considered in this paper and can be optimized for the two sub-packs separately.

B. SOC Balancing

To maintain good SOC balance in the pack, a rolling discharge approach is applied. This approach reasonably regulates $\vec{\boldsymbol{M}}_{\mathbf{1}}$ and $\vec{\boldsymbol{M}}_{\mathbf{2}}$ depending on the module SOCs $\chi_{(i,j)}$ to achieve them balancing. Its principle is similar to cell balancing [36], [37].

The SOC balancing process is described as follows. A battery state estimator firstly estimates $\chi_{(i,j)}$, $E_{(i,j)}$ and $R_{o,(i,j)}$ of all modules. The battery management system then descend-

ingly sorts $\chi_{(i,j)}$ in each battery sub-pack. The modules with high-level SOC in a sub-pack have higher discharge priority. Control input $\vec{\boldsymbol{M}}_{\mathbf{1}}$ and $\vec{\boldsymbol{M}}_{\mathbf{2}}$ are regulated corresponding to the discharge priority of the modules, and then the current allocations are predicted by (9). Simultaneously, the battery management system calculates all possible control input $\boldsymbol{U}_{\text{sys}}$ with considering battery system constraints (16). These processes can guarantee that the modules with high-levelSOCs operate at connection mode (Fig. 3a), and the modules with low-level SOCs operate at disconnection mode (3b). After a discharge period, the previous modules with high-level SOC would be turned into those with low-level SOC. Conversely, the previous modules with low-level SOC would be turned into those with high-level SOC. All modules will be in a rolling discharge/idle state though recurrent implementation of the processes. Consequently, the module SOCs in a sub-pack will be approximately balanced through the rolling discharging approach.

C. Power Allocation

During discharge mode IV, the power allocation between the two battery sub-packs must be regulated. In this study, the filtration-based control strategy is used to regulate them further. The filtration-based control strategy was initially developed in [38] for the HESS and extended to the semi-active HBS [24]. This method uses a low-pass filter to allocate the power, as expressed in (13).

$$\begin{aligned} \dot{P_f} &= -f_s P_f + f_s P_L \\ P_{\text{ref}} &= P_f + K\left(SOC_{\text{LTO}} - SOC_{\text{LTO,init}}\right) \end{aligned} \tag{13}$$

where f_s is the frequency of a low-pass filter, P_f is the filter power result (W), $SOC_{\text{LTO,init}}$ is the initial SOC of the LTO sub-pack, K is the gain of the difference between SOC_{LTO} and $SOC_{\text{LTO,init}}$, and P_{ref} is the LFP sub-pack reference power (W) expected to be achieved for the power allocation. As to the low-pass filter, f_s is represented by 10^{-3} Hz, and the value of K is 3000. Besides, the LFP reference power P_{ref} is limited within $0 \leq P_{\text{ref}} \leq P_L$ to avoid sub-packs charging each other.

However, the system configuration determines that the power allocation is discrete by regulating $\boldsymbol{U}_{\text{sys}}$. Thus, the battery management system can be designed as making power allocations fit as close as possible to P_{ref} by regulating $\boldsymbol{U}_{\text{sys}}$. The optimal output power of the LFP sub-pack can be expressed by (14).

$$\boldsymbol{U}^*_{\text{sys}} = \arg \min_{\boldsymbol{U}_{\text{sys}} \in \tilde{\boldsymbol{U}}_{\text{sys}}} \left[f_1(\boldsymbol{X}_{\text{sys}}, \boldsymbol{U}_{\text{sys}}, P_L) - P_{\text{ref}} \right]^2 \tag{14}$$

where $\boldsymbol{U}^*_{\text{sys}}$ is the optimal control input, and $\tilde{\boldsymbol{U}}_{\text{sys}}$ is the set of control input $\boldsymbol{U}_{\text{sys}}$. Thus, two battery sub-pack power distributions at input $\boldsymbol{U}^*_{\text{sys}}$ are shown in (15).

$$\begin{aligned} P_1 &= f_1(\boldsymbol{X}_{\text{sys}}, \boldsymbol{U}^*_{\text{sys}}, P_L) \\ P_2 &= f_2(\boldsymbol{X}_{\text{sys}}, \boldsymbol{U}^*_{\text{sys}}, P_L) \end{aligned} \tag{15}$$

Besides, the states that the battery sub-packs mutual charging need to be avoided to decrease unnecessary thermal energy generated, resulting in reduced battery system efficiency. Meanwhile, the output voltage needs to meet the limitation of the load voltage range to the greatest extent. The constraints of power allocation are expressed as (16).

$$\begin{aligned} 0 \le I_1 &\le I_{1,\max} \\ 0 \le I_2 &\le I_{2,\max} \\ V_L &\ge V_{L,\min} \end{aligned} \tag{16}$$

where $I_{1,\max}$ and $I_{2,\max}$ are the maximum discharge limitations for the LFP and LTO battery sub-packs, respectively, and $V_{L,\min}$ is the minimum load voltage limitation.

Equation (14) is a quadratic programming problem with the constraints (16), in which $S_1 = 1$ and $S_2 = 1$. This problem can be expressed as (17).

$$\begin{aligned} \boldsymbol{M}^*_{\text{sys}} &= \arg \min_{\boldsymbol{M}^*_{\text{sys}} \in \tilde{\boldsymbol{M}}_{\text{sys}}} \left[f_1(\boldsymbol{X}_{\text{sys}}, \boldsymbol{M}_{\text{sys}}, P_L) - P_{\text{ref}} \right]^2 \\ \text{subject to: } & 0 \le I_1 \le I_{1,\max} \\ & 0 \le I_2 \le I_{2,\max} \\ & V_L \ge V_{L,\min} \end{aligned} \tag{17}$$

where $\boldsymbol{M}_{\text{sys}} = [\vec{\boldsymbol{M}_1}^T, \vec{\boldsymbol{M}_2}^T]^T$, $\boldsymbol{M}^*_{\text{sys}}$ is the the optimal vector of $\boldsymbol{M}_{\text{sys}}$, and $\tilde{\boldsymbol{M}}_{\text{sys}}$ is the set of $\boldsymbol{M}_{\text{sys}}$. However, the elements of the vector $\boldsymbol{M}_{\text{sys}}$ are integer values because of the discrete-switched topology. Existing algorithms to solve the integer problem are time-consuming while needing a high-performance processor (e.g. genetic algorithm). Here, a 'special' enumeration is applies to solve this problem.

Based on (7) and (16), solutions have following conditions:

1) Assuming V_{LFP} is the voltage under the known positive power demand and only using the LFP battery sub-pack. Thus, E_2 satisify $E_2 \ge V_{\text{LFP}}$.
2) $E_1 \ge V_L$ and $E_2 \ge V_L$ under the constraints $I_1 \ge 0$ and $I_2 \ge 0$.
3) E_1 and E_2 also need to be greater than $V_{L,\min}$.

The processes of solving the quadratic programming problem are analysed as follows. The first step is to reduce the size of $\tilde{\boldsymbol{M}}_{\text{sys}}$ by the method of the proposed rolling dischrging

approach. The second step is to extract $\vec{\boldsymbol{M}}_{\mathbf{1}}$ and $\vec{\boldsymbol{M}}_{\mathbf{2}}$ which satisfy condition 3. The third step is to calulate V_{LFP} corresponding to each extracted $\vec{\boldsymbol{M}}_{\mathbf{1}}$, and each extracted $\vec{\boldsymbol{M}}_{\mathbf{1}}$ has some $\vec{\boldsymbol{M}}_{\mathbf{2}}$ which satisfy condition 2. Thus, the V_L, I_1, I_2, P_1 for each feasible combinations of $\vec{\boldsymbol{M}}_{\mathbf{1}}$ has some $\vec{\boldsymbol{M}}_{\mathbf{2}}$ can be calculated under filtering from step 1 to 3. Finally, through substituting I_1, I_2, P_1 into objective function (17), the optimal solution is the $\vec{\boldsymbol{M}}_{\mathbf{1}}$ and $\vec{\boldsymbol{M}}_{\mathbf{2}}$ which obtain minimum value in (17). Although it is still a complex algorithm, the size of $\tilde{\boldsymbol{M}}_{\mathrm{sys}}$ is reduced from $2^{113\times160}$ to only several hundred through the processes above. Finally, $J = \left[f_1(\boldsymbol{X}_{\mathrm{sys}}, \boldsymbol{M}_{\mathrm{sys}}, P_L) - P_{\mathrm{ref}}\right]^2$ can be calculated for each $\tilde{\boldsymbol{M}}_{\mathrm{sys}}$ processed. The $\boldsymbol{M}^*_{\mathrm{sys}}$ which can obtain the smallest J is selected as the input of $\vec{\boldsymbol{M}}_{\mathbf{1}}$ and $\vec{\boldsymbol{M}}_{\mathbf{2}}$.

V. Simulation Results and Analysis

A. Simulation Environment and System Configuration

In the proposed HBS evaluation of this study, a series of simulations and analyses are performed based on repeated typical EV power demand on Worldwide harmonised Light vehicles Test Cycles (WLTP) for Class 3 vehicles. Its speed profile is shown in Fig. 6 [39]. Furthermore, parameters of the EV (i.e., Nissan Leaf) are adopted, as listed in Table V [40]. More details of the dynamics model of the EV can be found in [25].

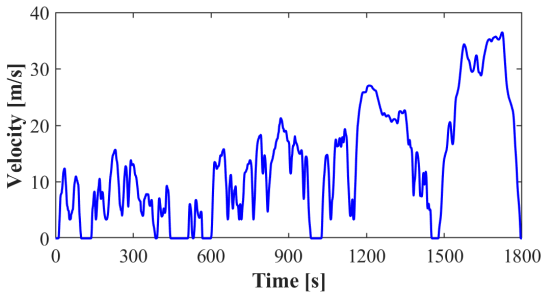

Fig. 6. Speed profile of the World harmonized Light vehicles Test Cycles (WLTP)

In the system, the parameters and characteristics of the selected LFP and LTO battery cell are shown in Table III and Fig. 5, respectively. The system adopts a configuration similar to the optimised energy ratios of the LTO and LFP battery sub-packs in [20]. A control group of the LFP battery system is established to compare the performances between the HBS and the LFP system. Furthermore, the nominal and minimum voltages are set as 360 V and 250 V, respectively. The HBS needs to provide energy to satisfy a driving distance of approximately 300 km. The HBS configuration and a control group (only LFP battery system) are listed in

Table VI, where 'LFP(HBS)' and 'LTO(HBS)' are the configulations of the sub-packs LFP and LTO in the HBS, and 'LFP system' is the only LFP battery system.

TABLE V
PARAMETERS OF THE EV

Parameters	Value
Mass (kg)	1580
Width (m)	1.788
Height (m)	1.530
Drag coefficient	0.29
Rolling resistance coefficient	0.015
Vehicle average efficiency	0.85

TABLE VI
THE HBS AND THE LFP SYSTEM CONFIGURATIONS

Parameters	LFP(HBS)	LTO(HBS)	LFP system
Serial Number	113	160	113
Parallel Number	12	4	16
Nom. voltage (V)	361.6	368	361.6
Capacity (kWh)	43.4	19.1	61.4

Besides, the maximum discharge limitation for $I_{1,\max}$ and $I_{2,\max}$ are 132 A and 434 A, respectively, based on the battery cell characteristics (Table III) and the HBS configuration (Table VI). The simulation environment is MATLAB/Simulink.

B. Simulation Results

Simulation results for power allocation under the WLTP drive cycle are shown in Fig. 7. Initially, the battery system runs in discharge mode III and mechanical braking mode at high-level SOC_{LFP} and SOC_{LTO}. With a SOC_{LTO} decrease, the system turns into discharge mode IV and regenerative braking mode I. The two battery sub-packs are coordinated discharging, and the LTO battery sub-pack starts to absorb energy from regenerative braking. During the period of coordinated discharging, the LTO sub-pack undertakes most of the power at high power

demand, making the LFP sub-pack work within a medium power range. When the SOC_{LFP} and SOC_{LTO} are close to the SOC lower bound, the system still runs in discharge mode IV and regenerative braking mode.Similarly, the LTO sub-pack is allocated a part of power demand at high power requirements. However, the LFP sub-pack output more power during this period. At the end of discharging processes, the system works in discharge modes I or II to protect two battery packs from over-discharges. Meanwhile, when normalising the battery cell current to the C-rate and compared to the single LFP battery system, the LFP battery sub-pack in thg HBS undertakes the lower current, as shown in Fig. 7(h). Consequently, simulation results verify that this topology can meet the power allocation requirement and decrease the LFP sub-pack power and current at high power demands.

Furthermore, the proposed topology can flexiably allocation the tow battery sub-packs' power. In Fig. 8, the expected powers for the two battery sub-packs are generated by Table IV, (13) and (14). Fig. 8(a) and (b) demonstrate that differences of the expected and actual powers in the two battery sub-packs are relatively small. To further compare the errors of the power allocation, Absolute errors between expected and actual power is used to assess its effectiveness, as expressed in (18).

$$P_{\mathrm{error}} = \left| P_{\mathrm{act}} - P_{\mathrm{exp}} \right| \tag{18}$$

where P_{act} and P_{exp} are the actual power and expected powers (kW), P_{error} is absolute errors between expected power and actual power (kW).

Fig. 8 (c) and (d) demonstrate P_{error} for LFP and LTO battery sub-packs, respectively. Errors can remain within 1.5 kW while allocating the power between two battery sub-packs. The errors within 1.5 kW are acceptable because the DC/DC converter also has errors within 5% when regulating the power allocation [41]. This means power distribution errors has $0 \sim 2$ kW when using DC/DC converter in this battery system. Therefore, the proposed topology has similar performance in flexibly regulating power allocation as the conventional HBS with DC/DC converter.

C. SOC Balancing

The results of SOC balancing processes are demonstrated in Fig. 9, where differences between the maximum and minimum SOCs of modules in the LFP and LTO battery sub-packs are defined as ΔSOC_{LFP} and ΔSOC_{LTO}, respectively. The battery system initially runs in discharge mode III and mechanical braking mode, and only the LTO battery sub-pack

participates in the operation, and all modules in the LTO battery sub-pack are discharged or charged. Thus, SOC_{LFP} and SOC_{LTO} maintain balance. Then, the module switches start allocating power (discharge mode IV), resulting in an unbalanced trend between modules. Simultaneously, the rolling discharging approach controls the module modes $\vec{\boldsymbol{M}}_{\mathbf{1}}$ and $\vec{\boldsymbol{M}}_{\mathbf{2}}$ to prevent the unbalanced trend from continuing to expand and maintains ΔSOC fluctuating within a small range. The simulation results show that ΔSOC_{LFP} and ΔSOC_{LTO} fluctuate within the range of $0 \sim 0.01\%$ and $0 \sim 0.1\%$ in the LFP and LTO battery sub-packs, respectively. It is verified that the topology can maintain the SOC balancing between modules in a sub-pack when the module currents are inconsistent.

The system can also balance the modules in battery sub-packs under initial module SOCs are unbalanced. It is assumed that initial module SOCs $\chi_{(i,j)}$ are randomly distributed within the range of 10% based on 80% of initial SOC_{LFP} and SOC_{LTO}. The results of the SOC balancing process is demonstrated in Fig. 10. During the SOC balancing process, both $\Delta SOC_{\mathrm{LFP}}$ and $\Delta SOC_{\mathrm{LTO}}$ decrease at discharge mode IV. The LTO battery sub-pack first reaches balancing at approximately 2000 seconds and then remains balance. The LFP battery sub-pack achieves the balancing slowly, but it can also remain after reaching it. The reason of LFP battery sub-pack slowly reaching the balancing is the lower current flowing through the LFP batteries. Specifically, the proposed topology utilises the discrepancy of accumulated electric charge of each battery module by regulating the $\vec{\boldsymbol{M}}_{\mathbf{1}}$ and $\vec{\boldsymbol{M}}_{\mathbf{2}}$ in the two sub-packs to make up for the difference of modules SOCs. Thus, the SOC balancing speed depends on the charging and discharging rate at discharge mode IV.

VI. Conclusion

A novel discrete-switched topology used in the HBS with LFP and LTO batteries has been proposed in this paper. The proposed topology is to utilise the discrete-switched structure for replacing the expensive and bulky DC/DC converter in the semi-active and active topology of the HBS. This study has explored a feasibility approach that simplifies battery system hardware at the expense of a more complex control algorithm. Simulation has verified the topology with the similar performance of regulating power allocation as the existing topology with DC/DC converters, ensuring that SOCs remain broadly balanced throughout discharge.

In this study, the topology is demonstrated in detail, and the system is modelled for explaining the power allocation method. A management strategy is then developed to meet the power allocation regulation between two batteries and balance SOCs in each sub-pack. A case study with the WLTP Class 3 driving cycle is implemented in MATLAB/Simulink.

Simulation results verify that this topology can allocate power flexibly (similar to an HBS with DC/DC converter). In addition to similar features to the conventional HBS, the proposed topology also has the following advantages:

1) The power electronics cost of the proposed topology is much cheaper than the conventional HBS with DC/DC converters. In the case study, the power electronics cost of the proposed topology is £383.6 compared to £2216.1 of the conventional semi-active topology under the same battery system configuration.
2) The topology can integrate two functions of power allocation and SOC balancing. In the case study, the LFP modules are in balance to within 0.01% of each other. The LTO modules are balanced to within 0.1% of each other. SOCs in the pack end up in good balance with each other.

The intended scope of this work is a decription of the novel technology paper only focuses on proposing the novel topology and verifying it has advantages of cost and the flexible power allocation capability. However, in automotive applications, various factors in the HBS need to be considered, including thermal effects, battery state estimations under non-uniform cells, thermal properties, control algorithm optimization and robustness, as well as load properties (e.g. characteristics of motors and inverters). Therefore, these factors in the novel hybrid battery systems will be further explored in the future.

VII. Acknowledgement

The authors thank Innovate UK for partially funding this work. The research data from the project will be available at https://doi.org/10.17862/cranfield.rd.19375928; it is subject to an embargo due to the terms of a confidentiality agreement.

References

[1] S. M. Lukic, J. Cao, R. C. Bansal, F. Rodriguez, and A. Emadi, "Energy storage systems for automotive applications," IEEE Trans. Indus. Electron., vol. 55, no. 6, pp. 2258–2267, 2008. [Online]. Available: https://doi.org/10.1109/TIE.2008.918390

[2] G. Ren, G. Ma, and N. Cong, "Review of electrical energy storage system for vehicular applications," Renewable Sustainable Energy Rev., vol. 41, pp. 225–236, 2015. [Online]. Available: https://doi.org/10.1016/j.rser.2014.08.003

[3] Boston Consulting Group, "Batteries for electric cars: Challenges, opportunities, and the outlook to 2020," 2010.

[4] G. Mulder, N. Omar, S. Pauwels, M. Meeus, F. Leemans, B. Verbrugge, W. De Nijs, P. Van den Bossche, D. Six, and J. Van Mierlo, "Comparison of commercial battery cells in relation to material properties," Electrochim. Acta, vol. 87, pp. 473–488, 2013. [Online]. Available: https://doi.org/10.1016/j.electacta.2012.09.042

[5] J. F. Peters, M. Baumann, B. Zimmermann, J. Braun, and M. Weil, "The environmental impact of Li-ion batteries and the role of key parameters: a review," Renewable Sustainable Energy Rev., vol. 67, pp. 491–506, 2017. [Online]. Available: https://doi.org/10.1016/j.rser.2016.08.039

[6] Y. Miao, P. Hynan, A. Von Jouanne, and A. Yokochi, "Current Li-ion battery technologies in electric vehicles and opportunities for advancements," Energies, vol. 12, no. 6, p. 1074, 2019. [Online]. Available: https://doi.org/10.3390/en12061074

[7] J. Wang, P. Liu, J. Hicks-Garner, E. Sherman, S. Soukiazian, M. Verbrugge, H. Tataria, J. Musser, and P. Finamore, "Cycle-life model for graphite-LiFePO4 cells," J. Power Sources, vol. 196, no. 8, pp. 3942–3948, 2011. [Online]. Available: https://doi.org/10.1016/j.jpowsour.2010.11.134

[8] K. Wu, J. Yang, Y. Zhang, C. Wang, and D. Wang, "Investigation on Li4Ti5O12 batteries developed for hybrid electric vehicle," J. Appl. Electrochem., vol. 42, no. 12, pp. 989–995, 2012. [Online]. Available: https://doi.org/10.1007/s10800-012-0442-0

[9] A.-I. Stan, M. Swierczynski, D.-I. Stroe, R. Teodorescu, S. J. Andreasen, and K. Moth, "A comparative study of lithium ion to lead acid batteries for use in UPS applications," in Proc. 2014 IEEE 36th Int. Telecom. Energy Conf. (INTELEC). [Online]. Available: https://doi.org/10.1109/INTLEC.2014.6972152

[10] G. Mulder, N. Omar, S. Pauwels, M. Meeus, F. Leemans, B. Verbrugge, W. De Nijs, P. Van den Bossche, D. Six, and J. Van Mierlo, "Comparison of commercial battery cells in relation to material properties," Electrochim. Acta, vol. 87, pp. 473–488, 2013. [Online]. Available: https://doi.org/10.1016/j.electacta.2012.09.042

[11] Z. Song, H. Hofmann, J. Li, J. Hou, X. Han, and M. Ouyang, "Energy management strategies comparison for electric vehicles with hybrid energy storage system," Appl. Energy, vol. 134, pp. 321–331, 2014. [Online]. Available: https://doi.org/10.1016/j.apenergy.2014.08.035

[12] Z. Song, J. Li, X. Han, L. Xu, L. Lu, M. Ouyang, and H. Hofmann, "Multi-objective optimization of a semi-active battery/supercapacitor energy storage system for electric vehicles," Appl. Energy, vol. 135, pp. 212–224, 2014. [Online]. Available: https://doi.org/10.1016/j.apenergy.2014.06.087

[13] Z. Song, H. Hofmann, J. Li, X. Han, X. Zhang, and M. Ouyang, "A comparison study of different semi-active hybrid energy storage system topologies for electric vehicles," J. Power Sources, vol. 274, pp. 400–411, 2015. [Online]. Available: https://doi.org/10.1016/j.jpowsour.2014.10.061

[14] G. Ren, G. Ma, and N. Cong, "Review of electrical energy storage system for vehicular applications," Renewable Sustainable Energy Rev., vol. 41, pp. 225–236, 2015. [Online]. Available: https://doi.org/10.1016/j.rser.2014.08.003

[15] D. Yan, L. Lu, Z. Li, X. Feng, M. Ouyang, and F. Jiang, "Durability comparison of four different types of high-power batteries in HEV and their degradation mechanism analysis," Appl. Energy, vol. 179, pp. 1123–1130, 2016. [Online]. Available: https://doi.org/10.1016/j.apenergy.2016.07.054

[16] N. Devillers, S. Jemei, M.-C. Péra, D. Bienaimé, and F. Gustin, "Review of characterization methods for supercapacitor modelling," J. Power Sources, vol. 246, pp. 596–608, 2014. [Online]. Available: https://doi.org/10.1016/j.jpowsour.2013.07.116

[17] C.-S. Moo, K. S. Ng, and Y.-C. Hsieh, "Parallel operation of battery power modules," IEEE Trans. Energy Convers., vol. 23, no. 2, pp. 701–707, 2008. [Online]. Available: https://doi.org/10.1109/TEC.2007.914310

[18] A. F. Burke, "Batteries and ultracapacitors for electric, hybrid, and fuel cell vehicles," Proc. IEEE, vol. 95, no. 4, pp. 806–820, 2007. [Online]. Available: https://doi.org/10.1109/JPROC.2007.892490

[19] N. Karim, E. J. Cairns, and P. H. Vroomen, "Electrically rechargeable, dual chemistry, battery system for use in plug-in or hybrid electric vehicles," U.S. Patent 9 774 204, Sep. 26, 2017. [Online]. Available: https://www.google.com/patents/US9774204

[20] X. Zhang, H. Peng, H. Wang, and M. Ouyang, "Hybrid lithium iron phosphate battery and lithium titanate battery systems for electric buses," IEEE Trans. on Veh. Technol., vol. 67, no. 2, pp. 956–965, 2017. [Online]. Available: https://doi.org/10.1109/TVT.2017.2749882

[21] C. J. Hale, "Battery system comprising a control system," U.S. Patent 10 449 868, Oct. 22, 2019. [Online]. Available: https://www.google.com/patents/US10449868

[22] W. Li, H. Cui, T. Nemeth, J. Jansen, C. Ünlübayir, Z. Wei, L. Zhang, Z. Wang, J. Ruan, H. Dai et al., "Deep reinforcement learning-based energy management of hybrid battery systems in electric vehicles," Journal of Energy Storage, vol. 36, p. 102355, 2021.

[23] Brill Power, "Brill Power: Revolutionizing energy storage," company website, accessed January, 2022. [Online]. Available: https://brillpower.com

[24] J. Ye, W. Zhuang, and G. Yin, "Rule-filter-integrated control of LFP/LTO hybrid energy storage system for vehicular application," in Proc. 2019 IEEE 28th Int. Symp. Ind. Electron. (ISIE), pp. 1542–1547. [Online]. Available: https://doi.org/10.1109/ISIE.2019.8781508

[25] G. Li, W. Zhuang, G. Yin, Y. Ren, and Y. Ding, "Energy management strategy and size optimization of a LFP/LTO hybrid battery system for electric vehicle," SAE, Tech. Rep. 2019-01-1003, 2019. [Online]. Available: https://doi.org/10.4271/2019-01-1003

[26] U. Research and I. (2021), "'chimera: an intelligent battery management architecture for next-generation electric vehicle batteries using multiple cell chemistries," accessed May 26, 2022. [Online]. Available: https://gtr.ukri.org/projects?ref=48727

[27] B. U. Research and I. (2022), "'bellerophon rapid assembly and disassembly," accessed May 26, 2022. [Online]. Available: https://gtr.ukri.org/projects?ref=10017550

[28] R. Wegmann, V. Döge, and D. U. Sauer, "Assessing the potential of a hybrid battery system to reduce battery aging in an electric vehicle by studying the cycle life of a graphite NCA high energy and a LTO metal oxide high power battery cell considering realistic test profiles," Appl. Energy, vol. 226, pp. 197–212, 2018. [Online]. Available: https://doi.org/10.1016/j.apenergy.2018.05.104

[29] C. D. Rahn and C.-Y. Wang, Battery Systems Engineering. Wiley, 2013. [Online]. Available: https://doi.org/10.1002/9781118517048

[30] R. Sharma and H. Gao, "Low cost high efficiency dc-dc converter for fuel cell powered auxiliary power unit of a heavy vehicle," IEEE transactions on power electronics, vol. 21, no. 3, pp. 587–591, 2006.

[31] I. I. Rectifier, "Irf2204s lpbf product data sheet," accessed May 25, 2022. [Online]. Available: https://docs.rs-online.com/7bd0/0900766b813418b8.pdf

[32] A.-I. Stroe, M. Swierczynski, D.-I. Stroe, and R. Teodorescu, "Performance model for high-power lithium titanate oxide batteries based on extended characterization tests," in Proc. 2015 IEEE Energy Convers. Cong. Expo. (ECCE), pp. 6191–6198. [Online]. Available: https://doi.org/10.1109/ECCE.2015.7310528

[33] R. Jackey, M. Saginaw, P. Sanghvi, J. Gazzarri, T. Huria, and M. Ceraolo, "Battery model parameter estimation using a layered technique: an example using a lithium iron phosphate cell," SAE International, Tech. Rep. 2013-01-1547, 2013. [Online]. Available: https://doi.org/10.4271/2013-01-1547

[34] A. Fotouhi, D. J. Auger, K. Propp, S. Longo, and M. Wild, "A review on electric vehicle battery modelling: From lithium-ion toward lithium-sulphur," Renewable and Sustainable Energy Reviews, vol. 56, pp. 1008–1021, 2016. [Online]. Available: https://doi.org/10.1016/j.rser.2015.12.009

[35] Y. Ko and W. Choi, "A new SOC estimation for LFP batteries: Application in a 10 Ah cell (HW 38120 L/S) as a hysteresis case study," Electronics, vol. 10, no. 6, p. 705, 2021. [Online]. Available: https://doi.org/10.3390/electronics10060705

[36] D. W. Gao, Energy Storage for Sustainable Microgrid. Academic Press, 2015. [Online]. Available: https://doi.org/10.1016/C2014-0-04144-5

[37] F. A. Silva, "Power electronic converters and systems: Frontiers and applications [book news]," IEEE Ind. Electron. Magazine, vol. 10, no. 2, pp. 68–70, 2016. [Online]. Available: https://doi.org/10.1109/MIE.2016.2554842

[38] A. Jaafar, C. R. Akli, B. Sareni, X. Roboam, and A. Jeunesse, "Sizing and energy management of a hybrid locomotive based on flywheel and accumulators," IEEE Tran. Veh. Technol., vol. 58, no. 8, pp. 3947–3958, 2009.

[Online]. Available: https://doi.org/10.1109/TVT.2009.2027328

[39] T. Schuetz, Aerodynamics of Road Vehicles, 5th ed. SAE International, 2015.

[40] Nissan UK, "New Nissan LEAF price and specifications," accessed July 25, 2021. [Online]. Available: https://www.nissan.co.uk/vehicles/new-vehicles/leaf/prices-specifications.html#grade-LEAFZE1A-0|specs

[41] N. Mohan, T. M. Undeland, and W. P. Robbins, Power Electronics: Converters, Applications, and Design. Wiley, 2003.

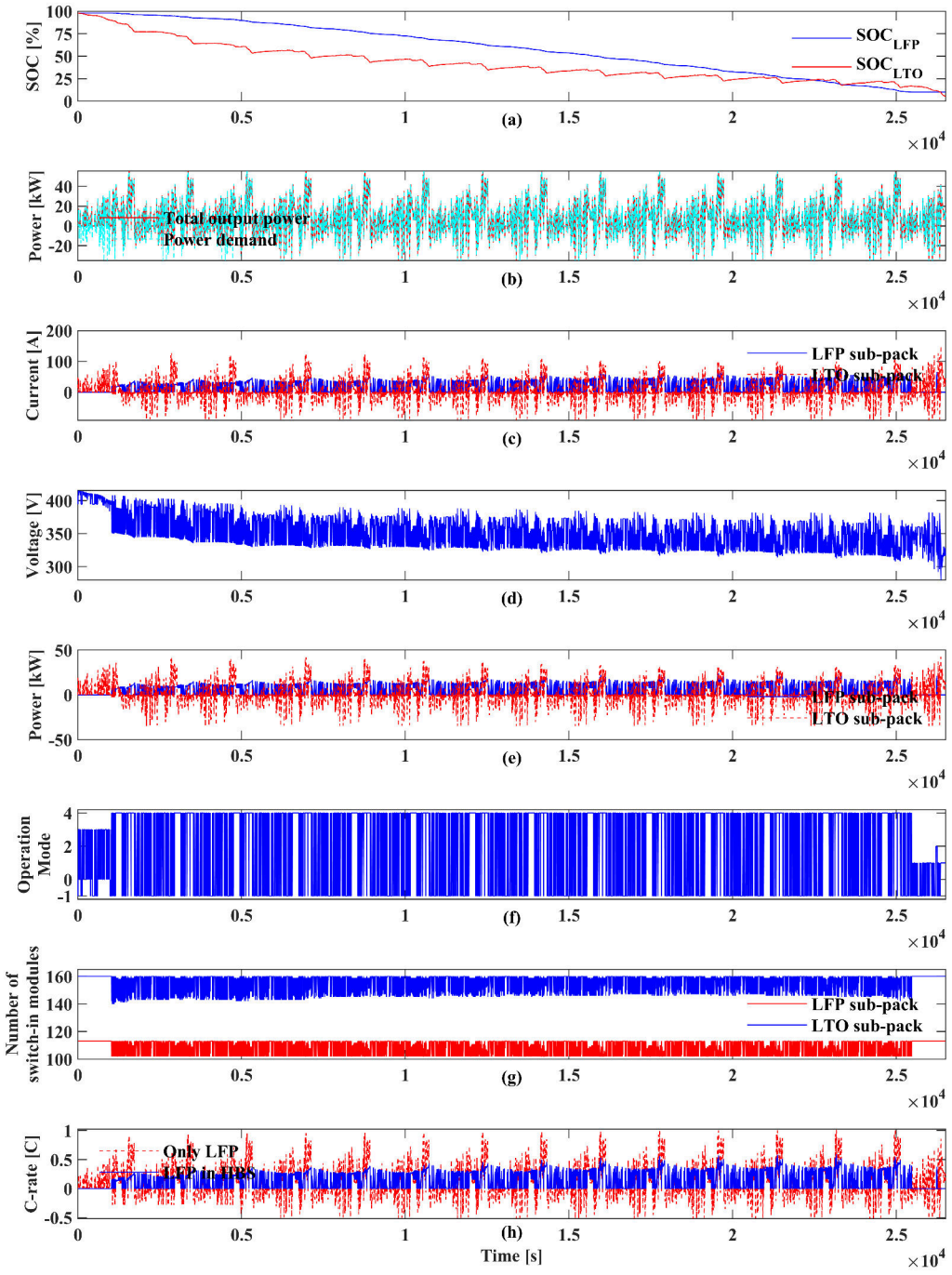

Fig. 7. Simulation results. (a) SOC for the LFP and LTO battery sub-packs. (b) Comparison between power demand and total output power for the HBS. (c) Current allocations of the two battery sub-packs. (d) Battery pack terminal voltage V_L. (e) Power allocations of the two battery sub-packs. (f) Battery system operation mode: The discharge modes are represented by $1--4$, mechanical braking mode is represented by 0, and regenerative braking modes are represented by -1, corresponding to Table IV. (g) Number of connection mode modules in the two battery sub-packs. (e) Comparison of Charge/discharge rate (C-rate) between the LFP battery sub-pack in HBS and the LFP battery system.

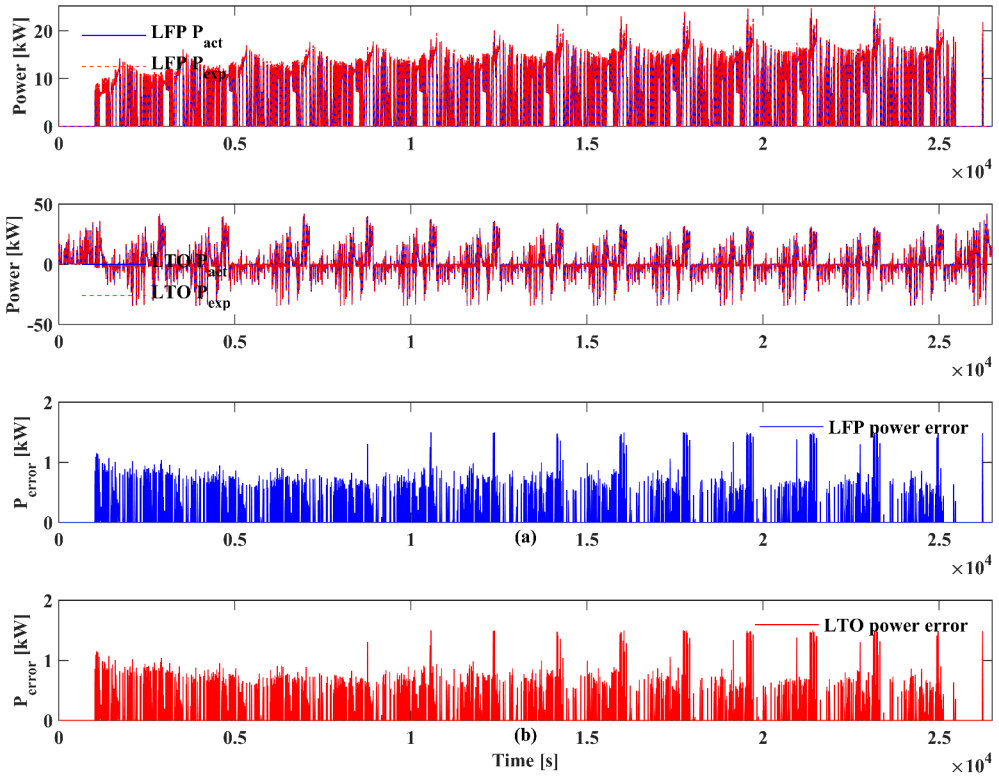

Fig. 8. Comparison between expected and actual power on: (a) P_{act} and P_{exp} for the LFP battery sub-pack, (b) P_{act} and P_{exp} for the LTO battery sub-pack, (a) P_{error} of the LFP battery sub-pack, (b) P_{error} of the LTO battery sub-pack.

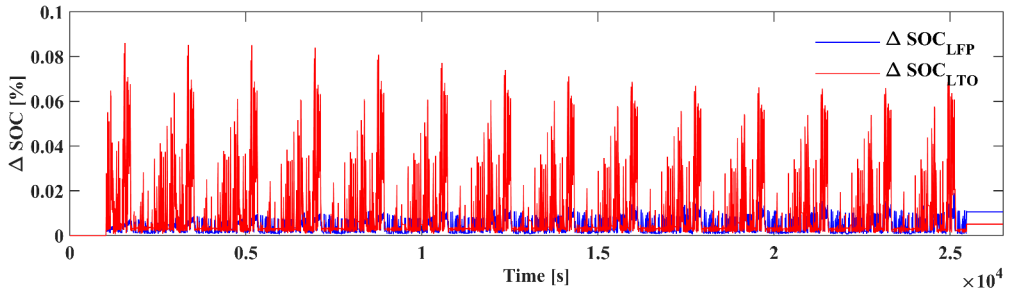

Fig. 9. The difference between the maximum and minimum SOCs of modules in the LFP and LTO battery sub-packs

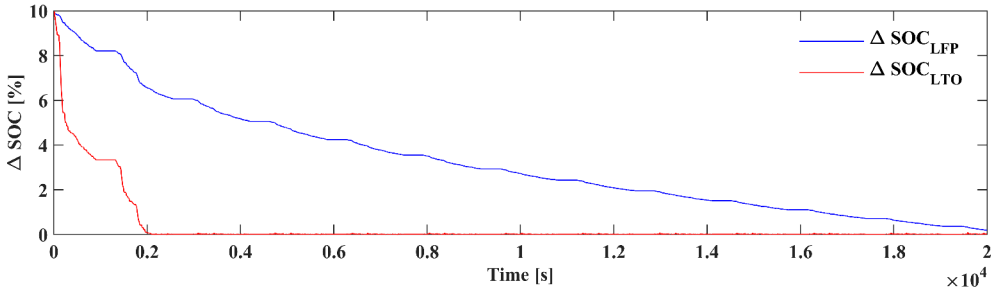

Fig. 10. Battery active balancing for LFP and LTO battery sub-packs under initial condition of unbalanced module SOCs

2022-07-12

A new topology for electric all-terrain vehicle hybrid battery systems using low-frequency discrete cell switching

Gong, You

IEEE

Gong Y, Auger DJ, Fotouhi A, Hale CJ. (2023) A new topology for electric all-terrain vehicle hybrid battery systems using low-frequency discrete cell switching. IEEE Transactions on Transportation Electrification, Volume 9, Issue 1, March 2023, pp. 609-621

https://doi.org/10.1109/TTE.2022.3190167